*IRACST – International Journal of Computer Networks and Wireless Communications (IJCNWC), ISSN: 2250-3501*
*Vol.9, No 4, Oct– Dec 2019*

# Kinematic phase lag variation between two robotic insect wings for controlling flight fluid dynamics

Will J. Maybury and Fritz-Olaf Lehmann*
*Department of Neurobiology, University of Ulm, Albert-Einstein-Allee 11, 89081 Ulm, Germany*
*Address for correspondence (e-mail: fritz.lehmann@biologie.uni-ulm.de)

*Accepted 30 September 2004*

**Abstract;** Flying insects with two sets of wings have to deal with the wake created by the beating of one set of wings passing over the beating of the other. Since the wings of insects like dragonflies may be moved independently of one another, the insects' fore- and hindwing stroke cycles can shift relative to one another. Since the impact of wing-wake interference is so dependent on the complex wake pattern created by the two beating wings, gauging the relevance of adjusting the phase relationship between fore- and hindwing stroke kinematics on overall lift generation is challenging in the flying animal. Using a dynamically scaled electromechanical insect model, we explore the impact of varying the fore- and hindwing stroke-phase relationship on the aerodynamic efficiency of each flapping wing under hovering flying circumstances. We observed that the forewing's performance is roughly consistent throughout a wide range of relative phase differences between fore- and hindwing stroke cycles, but the generation of lift by the hindwing may vary by as much as a factor of two. Raise of the rear wing

It seems that two distinct fluid dynamic phenomena—the annihilation of leading edge vortices and variations in the intensity and direction of the local flow vector—are responsible for the observed modulation. Surprisingly, when the motion of the hindwing precedes the forewing by about a quarter of the stroke cycle, the aerodynamic performance of the hindwing returns to that of the wing free from forewing wake influence. The phase-shift employed by locusts and certain species of dragonfly during ascent and forward flight is quite similar to the kinematic link between the hind- and forewings. The results of the tests corroborate the hypotheses that dragonflies and other insects with a functioning fourth wing may be able to adjust ipsilateral flight force generation via active neuromuscular regulation of fore- and hindwing stroke phase.

**Key words**: insect flight, aerodynamics, DPIV, leading edge vortex, wake, dragonfly.

## Introduction

Flying insects with two sets of wings have to deal with the wake created by the beating of one set of wings passing over the beating of the other. Since the wings of insects like dragonflies may be moved independently of one another, the insects' fore- and hindwing stroke cycles can shift relative to one another. Since the impact of wing-wake interference is so dependent on the complex wake pattern created by the two beating wings, gauging the relevance of adjusting the phase relationship between fore- and hindwing stroke kinematics on overall lift generation is challenging in the flying animal. Using a dynamically scaled electromechanical insect model, we explore the impact of varying the fore- and hindwing stroke-phase relationship on the aerodynamic efficiency of each flapping wing under hovering flying circumstances. We observed that the forewing's performance is roughly consistent throughout a wide range of relative phase differences between fore- and hindwing stroke cycles, but the generation of lift by the hindwing may vary by as much as a factor of two. Raise of the rear wing

It seems that two distinct fluid dynamic phenomena—the annihilation of leading edge vortices and variations in the intensity and direction of the local flow vector—are responsible for the observed modulation. Surprisingly, when the motion of the hindwing precedes the forewing by about a quarter of the stroke cycle, the aerodynamic performance of the hindwing returns to that of the wing free from forewing wake influence. The phase-shift employed by locusts and certain species of dragonfly during ascent and forward flight is quite similar to the kinematic link between the hind- and forewings. The results of the tests corroborate the hypotheses that dragonflies and other insects with a functioning fourth wing may be able to adjust ipsilateral flight force generation via active neuromuscular regulation of fore- and hindwing stroke phase. Wing kinematics like stroke amplitude and angle of attack often vary along with phase alterations (Reavis and Luttges, 1988; Wakeling and Ellington, 1997). This is why many experiments (Kesel, 2000; Kliss et al., 1989; Newman et al., 1977; Okamoto et al., 1996; Saharon and Luttges, 1987; Somps and Luttges, 1985) and theoretical studies (Kesel, 2000; Kliss et al., 1989; Newman et al., 1977; Okamoto et al., 1996; Saharon and Lutt (e.g. Azuma et al., 1985; Wang et al., 2003). The aerodynamics of a dragonfly were experimentally modeled in 2D by Savage et al. (1979), who dragged a single model wing on a carriage through the air and calculated the forces exerted by the wing's wake using inviscid flow theory. In order to explore

vortex shedding, Kliss et al. (1989) employed an oscillating flat plate at a 90° angle of attack. They discovered that the stroke length plays a crucial role in reducing the occurrence of total flow separation during the wing's translation. Saharon and Luttges (1987, 1988, 1989) conducted a series of detailed experiments to show that a mechanically driven dragonfly can create vortices under 3D flapping settings, and they defined eight primary vortices that are formed during each wing beat cycle. Maximum wing-wake interaction was shown to be negatively affected by the interference between the wakes of the back and front wings in the majority of instances studied. Vortices seemed to merge under certain flapping situations, and the flow wing-wake patterns were distinct for 90, 180, and 270 degree stroke-phase connections. When the phase connection was changed, a quantitative examination of the vortex displacement in the wake showed that the speed of certain vortices shed in the wake changed (Saharon and Luttges, 1989). The aforementioned investigations have not, however, explicitly assessed the aerodynamic forces generated by the flapping fore- and hindwing, nor have they quantified changes in leading edge vorticity and local flow conditions in response to varying kinematic phase angles.

Using a 3D robotic dragonfly model simulating hovering conditions at intermediate Reynolds number, we were able to experimentally investigate the complex wing-wake interaction in four-winged insects and evaluate the functional significance of stroke-phase modulation on wake structure, aerodynamic force production, and lift-to-drag ratio. To quantify vorticity and vortical flow structures at the wings, including the structures shed into the wake, we recorded the velocity field surrounding the flapping wings using Digital Particle Imaging Velocimetry (DPIV) while adjusting the kinematic phase shift.

## Materials and methods

Using a dynamically scaled electromechanical model of the right side of a four-winged flyer, we simulated the wing-wake interaction of a dragonfly in hovering flight in order to experimentally evaluate the global effects on wing lift force due to modulation of fore- and hindwing stroke phase in four- winged flight.

bug, while using the standard kinematic setup we'll go through below (Fig. 1B,D). We measured the instantaneous aerodynamic force output by equipping the model wings with 6-DoF force transducers and then systematically changing the kinematic phase connection between the wings by 2.5% of the stroke cycle. For the two kinematics phase changes that provide the greatest and lowest variation in hindwing lift at two important periods during the stroke cycle, we measured the forces acting on the wing and also used 2D-DPIV to quantify the flow features surrounding the wing.

Designing a standardised method of wing motion and control

It seems to be difficult to characterize a typical dragonfly kinematics due to the wide variety of stroke patterns utilized by dragonflies for weight balance and maneuverability (Norberg, 1975; Rüppell, 1989). During forward and rising flight, some species of dragonfly beat their wings with a nearly horizontal stroke plane (Wakeling and Ellington, 1997; Fig. 1A), while other species beat their wings at a steep angle (Azuma and Watanabe, 1988; Wang et al., 2003). Stroke amplitude and frequency in dragonflies may vary from 50° to 150° and 27Hz to 73Hz, respectively, to generate flying forces (Azuma and Watanabe, 1988; Rüppell, 1989).

It is because of this variety that many writers have attempted to describe dragonfly kinematics physically and analytically. While the stroke amplitude, frequency, and aspect ratio were all modeled for the oscillating flat plate scenario (Kliss et al., 1989), other elements of dragonfly wing motion, such as wing-wake interaction, were not modeled. Aerodynamic flow patterns generated over a wide range of Reynolds numbers (Re) from 10 to 4300 were also compared in this research. Norberg's kinematic data of freely flying dragonfly Aeschna was utilized in Savage's physical model of a hovering dragonfly (Savage et al., 1979). (Norberg, 1975). But, unlike real wings, this model did not rotate its wing between upstroke and downstroke; instead, it translated the wing. Saharon and Luttges' (1988, 1989) more complex "pitching-plunging" dragonfly model included the flapping of two ipsilateral wings on an angled stroke plane with a 90° stroke amplitude. With this model, the authors changed the decreased frequency, which led to variations in Re and three different phase angles between the fore- and hindwing (Saharon and Luttges, 1989). Dragonfly wings and bodies were studied for their aerodynamic qualities in a wind tunnel in 2D circumstances (Kesel, 2000; Okamoto et al., 1996). This later research assessed the influence of angle of attack (dragonfly wing), camber, thickness sharpness of the leading wing edge, and surface roughness (model wing) on force generation at Re=1000-10000 using a glider equipped with both dragonfly wings and flat plates.

For the current investigation, we designed a generic kinematic pattern to represent kinematic phase changes comparable to those described for dragonflies without having to account for an overwhelming number of

kinematic factors (Fig. 1B). As for the horizontal wing,trajectories were derived from a simple sinusoidal function, which was chosen because of a finding in previous studies that the first harmonic of a Fourier series gives a good representation of the stroke cycle of freely flying dragonflies (Azuma and Watanabe, 1988; Wakeling and Ellington, 1997; Wang et al., 2003). We used a constant angle of attack during wing translation with a feathering angle of 45° at mid stroke, which is similar to values reported previously (Azuma and Watanabe, 1988; Fig. 2B). This angle is the optimum lift angle of a translating wing free from wake interference and is within the range of data published for dragonflies (Dickinson et al., 1993; Rüppell, 1989). The stroke amplitude of 100° that we used is near the average measured for both the fore- and hindwing motion in dragonflies flying at various flight speeds (Wakeling and Ellington, 1997). The flapping frequency of the robotic wings was 533 mHz.

We chose to stack the wings vertically, which seems to be sufficiently close to the orientation of wing hinges presented by a freely flying dragonfly with a near vertical mean thrust vector (Fig. 1A,B). In this respect our tandem model with vertical aligned wings differs from other dragonfly models in which the wing hinges are aligned horizontally, yielding a 'front' and a 'rear' wing rather than an 'upper' and a 'lower' wing (Saharon and Luttges, 1987, 1988). For this reason, our model only covers a limited aspect of four-winged insect flight. It is not intended to explain *per se* the various types of wing–wake interaction assumed during the various forward and hovering flight conditions found in freely flying dragonflies. If not stated otherwise, fore- and hindwing hinges in our robotic model were separated vertically by 1.3 mean forewing chord lengths, i.e. the closest distance between the wings at which the wings did not touch physically during flapping at the various kinematic phase relationships (Fig. 1C). In accordance with the stroke kinematics used for an analytical dragonfly model, we chose a symmetrical wing rotation during the ventral and dorsal stroke reversal, in which the midpoint of rotational duration occurs when the wing reverses its translational direction (Wang, 2000a). A wing rotating symmetrically starts rotating before and finishes after it has reversed its flapping direction, which may minimize rotational lift because at that time translational wing velocity is smallest. To minimize inertial load produced by rotational moments in our generic kinematic pattern, wing rotation followed a sinusoidal velocity profile. The onset of wing rotation relative to stroke reversal, expressed as a fraction of the total wing cycle time, $\tau_0$, was –0.1, indicating that wing rotation begins 10% of the stroke period prior a stroke reversal. Flip duration, $\Delta\tau$, was 0.2, indicating that wing rotation ends 10% after the stroke reversal (for nomenclature, see Sane and Dickinson, 2001a). The kinematic pattern we used in this study produces lift due to wing rotation equivalent to 3.2% of total lift production by the hindwing free from forewing wake interference. We estimated rotational lift contribution from total lift by subtracting the 'quasi-steady' lift estimate during wing translation that was calculated using a conventional 'quasi-steady' analytical model, as suggested by Dickinson et

al. (1999). (1999). Overall, the current investigation suggests that the significant variability in recorded hindwing lift generation reflects aerodynamic processes during wing translation, rather than changes in rotational circulation during the stroke reversals.

Six servo motors, controlled by custom software created in Visual C++.NET (Microsoft) on a desktop PC, moved the two model wings. The computer was fitted with a 16-channel analog-to-digital data acquisition board (6036E, National Instruments, Austin, TX, USA) for recording force data and a 24-bit digital interface card (6503, National Instruments) for controlling the motion of the servo motors via a micro-controller, allowing for simultaneous force data recording and wing motion control (Fig. 1C). At its fastest, we were able to update the motor assembly's angular location at a rate of 67 Hz (0.015 ms), while the force was sampled at a rate that was around 12 times faster, at 800 Hz. Problems may arise during the wing motion of robotic wings if the real power needs for wing motion exceed the power provided by the driving motors. This is particularly true when the wings are subjected to a large inertial load, such as during a start-up acceleration. We updated the servo motors to electronically monitor their internal angular position, which is physically dictated by the angle of the motor main shaft driving the wing, so as to eliminate any potential for power limits of the motor assembly to introduce noise into our force measurements. Prior to each set of experiments, we performed a control procedure in which we compared the actual angular position of each servo motor with the programmed wing angles and adjusted the power supply to the motors or the frequency at which the wings flapped until the two sets of kinematics were indistinguishable. The high power demand for wing flapping was a primary problem that restricted the maximum flapping speed and, therefore, Re of our model wings.

Wing flexing and bending may also cause kinematic changes in wing motion, in addition to power limits. Furthermore, inertial peaks may be created by wing flexing, adding complexity to the recorded force traces. A significant wing flex might contribute short acceleration/deceleration components to the overall wing acceleration/deceleration profile that is created by the translational and rotational wing motion, even though the inertial forces produced during these times are very minor (see below and Fig. 2A). As shown in Fig. 2B, the maximum combined aerodynamic and inertial stress on the trailing wing during each mid-halfstroke is between 0.4 and 0.6 N. We statically loaded the wing in air with small weights placed at a distance of two-thirds wing length on the upper wing surface or at the wing tip, and

we measured the deflection of the wing at both locations to get a ballpark estimate of the magnitude of wing flexing at the various times of the stroke cycle (Fig. 1D). Putting in the wing at the wing tip is thought to produce a rather conservative estimate because the main force vector during wing translation is thought to act close to the two-thirds wing position. The results show that with an average load of 0.3 N, which is equal to the average force measured throughout the entire stroke cycle, fore- and hindwing solely flex approximately 1.0 mm at two-thirds distance from the wing holder, and up to 1.7 mm under the maximum load of 0.5 N that occurs approximately at mid-halfstroke. Due to the sinusoidal velocity profile during wing translation, however, we assume that the wing builds up and releases its deflection more gradually at the beginning and the end of each halfstroke, respectively, which should in turn minimize sudden accelerations and thus high inertial peaks. In sum, we feel rather confident that the measured alteration in force development due to the various kinematic phase shifts between fore- and hindwing are not primarily caused by extensive wing flexion but are likely to represent aerodynamic alterations due to wing–wake interaction.

*Force measurements*

The 2 mm thick Plexiglas wings were modeled after the fore and hind wings of the dragonfly Polycanthagyna melanictera Selys. We determined the overall wing length as the horizontal distance from the gear box's rotating axis to the wing's leading edge, since the wing's angular velocity is proportional to the blade element's proximity to the axis. Taking into account the gear box, force sensor, and wing holder, the overall wing length was 190 mm with an aspect ratio of 6.8 while the wing length of the rear of the aircraft was 185 mm with an aspect ratio of 7.4. (Fig. 1C). Sensu strictu (without the wing holding, force sensor, and gear box), however, the upper forewing was only 135 mm in length (aspect ratio=3.6; Fig. 1C), while the lower hindwing was 140 mm in length (aspect ratio=4.2). Each wing was attached to a robotic hinge that allowed for three degrees of freedom and had a single point of origin.

We hypothesized that the flow conditions experienced by a four-winged insect during hovering flight would be different from those experienced during continuous forward flight, and we modeled such a scenario. In insects, "steady motion" is the result of the insect's body traveling through the air at a constant speed, whereas "unsteady motion" is the result of the wing moving back and forth with respect to the insect's body. Hence, the advanced ratio and the lowered frequency may be used to determine whether velocity component (free stream owing to body motion or wing flapping) dominates the incidence flow on the wing. Analytical modeling in the "quasi-steady" regime and the design of dynamically scalable robotic hinges need both numbers. Yet, as we simulated a hovering flying situation, all flow components acting on the two wings are created by the motion of the wings themselves, leading to a zero advance ratio and an infinite reduced frequency.

Both of the wings, covered with scales, were submerged in a glass tank measuring 0.6 by 0.6 by 1.2 meters filled with white oil used in the pharmaceutical industry (density: 0.88 103 kg m-3; kinematic viscosity: 120 cSt). The tank was designed such that it would have the fewest possible walls and

The ground effects were determined using a set of equations developed from a robotic wing flying in oil at a comparable pace (Dickinson et al., 1999). Experiments were run twice to get readings from both wings, using a customized force/torque sensor (Nano17, ATI, Apex, NC, USA) mounted to the base of each wing in turn. The three axes of the wing were measured for shear forces and moments by the sensor. Using commercial Active-X controls (ATI) and software built in Visual C++.NET, we were able to translate forces recorded normal and parallel to the wing surface into lift and drag. On average, we logged data from six consecutive stroke cycles. Since the downwash velocity is lowest during the first stroke cycle, it has been shown that somewhat more forces are generated (Birch and Dickinson, 2001). To keep the data analysis manageable, we merely averaged four stroke cycles (cycles 2–5).

Keeping track of the amount of lift exerted on the parked wing at each stage of the wing's stroke. Since we assumed that the whole mass of the wing, mw, including the mass of the wing holder, is concentrated in the center of wing mass, we were able to analytically determine the contribution of inertial forces attributable to wing mass. We have placed a red dot in the middle of each wing in Fig. 1C to represent the wing's center of mass. Though the wing holder's mass is relatively close to the mounting surface of the force sensor, to which all forces and moments refer, its total mass of about 7.0 g is roughly 54% of the mass of the larger forewing and 62% of the mass of the smaller hindwing, and so should be considered for inertial effects. Inertial forces during flapping flight in the horizontal plane are proportional to the initial moment of wing mass m1, as stated by Ellington (1984a), which is a modified formulation of equation 12 in Ellington (1984c) derived for hovering flying insects presenting a horizontal stroke plane (Lehmann and Dickinson, 1998). The density of the mineral oil is, the stroke amplitude is the angle that the wings cover during wing translation, n is the stroke frequency, R is the wing length, S is the total wing area, (d/dt) is the mean square of the dimensionless wing velocity, and r2 is the non-dimensional radius of the second moment of area that characterizes wing shape (for nomenclature, see Ellington, 1984d). The mean square of the dimensionless wing velocity for a sinusoidal velocity pattern in wing translation is 19.7. (Lehmann and Dickinson, 1998) Our hypothetical dragonfly has a forewing nondimensional radius of 0.36 and a hindwing nondimensional radius of 0.38. The force coefficients are a way to describe a fusion of several types of circulation into a single quantity, such as the Kutta-lift, leading edge vorticity, and rotational circulation, and even a potential wake-capture momentum transfer (Dickinson et al., 1999).

*Wing inertia and added mass effects*

In real and model wings the forces at the wing base consist of at least three different components: (i) aerodynamic forces due to both the pressure distribution around the wing and viscous forces in the fluid, (ii) inertial forces due to wing and added mass acceleration, and (iii)

gravitational forces. The gravitational component on the force sensor is due to the mass of the wing and was subtracted from the measured forces by

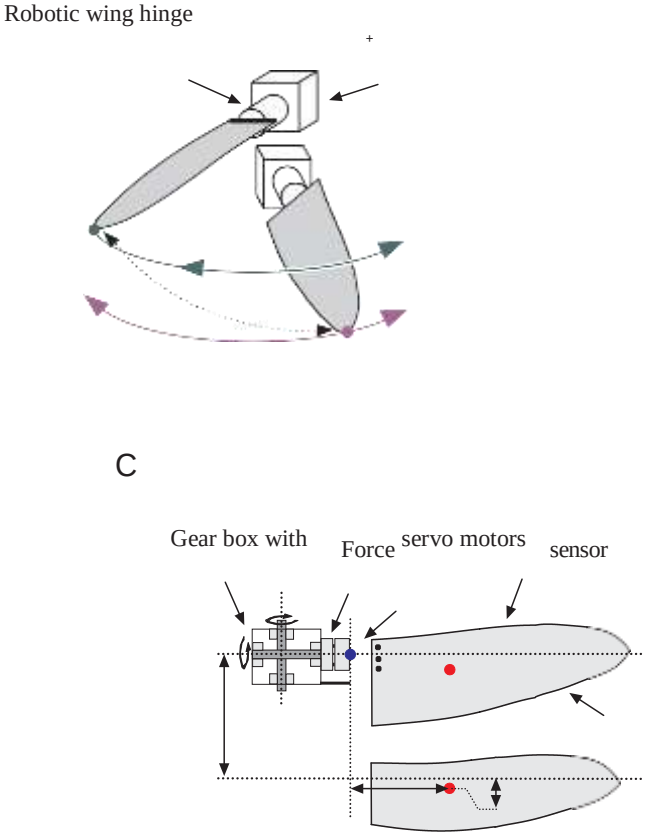


Fig. 1. Wing beat kinematics of a dragonfly, set-up of the robotic wing hinge, and mechanical properties of the model wings as used in this study. (A) Diagram showing wing tip path of fore- (green) and hindwing (purple) and orientation of a freely flying dragonfly with near vertical thrust vector. Body orientation, location of the wing hinges and wing tip path were plotted after data published by Wakeling and Ellington (1997). In this kinematic study advance ratio, defined as the ratio between forward and wing flapping speed, was 0.44. Due to the steep body angle with respect to the horizontal, the wing hinges are aligned almost vertically and thus similar to the alignment of the robotic wing hinges shown in (B). (B) Schematic diagram of the robotic dragonfly setup, modeling aerodynamic characteristics on one side of the functionally four- winged insect with the forewing and hindwing wingtip trajectories of our generic dragonfly kinematics superimposed (see Materials and methods for details). The kinematics used during fore- and hindwing motion is identical in all experiments, yielding 100° stroke amplitude and symmetrical wing rotation at dorsal and ventral stroke reversal. Kinematic phase shift is the temporal offset between fore- and hindwing motion.
(C) The shape of the robotic forewing and hindwing used. The wings are driven by servo motors mounted in a gear box that controls back/forth, up/down and rotational wing motion. Forces and moments acting on the wing during motion are measured on the surface mid point of the force sensor (blue circle). The center of gravity of the wing including the mass of the wing's holder is indicated by a red circle, respectively. $l_x$, length of the horizontal moment arm for the wing's center of gravitiy; $l_y$, length of the vertical moment arm between the wing's center of gravitiy and the wing's rotational axis. (D) Wing deflection due to bending moments under static load of the plexiglas model forewing (orange, red, black) and hindwing (cyan, green, blue). Deflection during load was measured at two distinct positions on the wing at two-third wing length (orange, cyan) and the wing tip (red, black, green, blue). To load the wing, small metal weights were placed on the upper wing surface either at two-third distance from the wing base (**, red, green, cyan, orange) or on the wing tip (*, black, blue). The vertical gray line indicates approximately mean force (0.3 N) measured throughout one complete stroke cycle on the wings during flapping motion. Horizontal gray area shows the range of deflections for fore- and hindwing, assuming the wing is loaded with mean force. The pictogram illustrates the measurement procedure showing wing holder and the wing seen parallel to the wing's surface.

Moreover, the smoke traces used to visualize the wake in the 3D dragonfly model suggested constructive vortex fusion that might amplify downwash patterns and enhance vortex persistence of the wings. In contrast, in the present robotic model we did not observe that vortices with the same spin fused in the wake, but found instead that hindwing LEV stability and persistence appears to be influenced by trailing edge vorticity shed from the forewing.

The robotic dragonfly model suggested by Saharon and Luttges (1988) differs from the present hovering model in several respects. First, Saharon's and Luttges' model was placed in a wind tunnel with a freestream velocity of 76 cm $s^{-1}$. From the data provided, we calculated a mean wing tip velocity of 540 cm $s^{-1}$ that results in an advance ratio of approximately 0.14, whereas advance ratio in the present model is zero.

Fig. 10. Modulation of hindwing lift depends on the vertical distance between fore- and hindwing wing hinges. The traces show lift modulation similar to Fig. 3C for various distances between the wings measured in mean chord width *c*, while phase lag systematically varied between –50% (forewing leads by a half stroke cycle) and 50% (hindwing leads by a half stroke cycle). Aspect ratio of the two identical wings=2.7, stroke amplitude=120°, flapping frequency= 666 mHz, wing rotation symmetrical, *Re*=137.

we visualized in the wake are thus similar to the two major vortical structures found in other physical insect models, mimicking a 3D complete stroke cycle in the horizontal: a large starting vortex shed at the beginning of each half stroke and a leading edge vortex during wing translation (Figs 5 and 6; Birch and Dickinson, 2001; Dickinson et al., 1999; Ellington et al., 1996). Due to the complex flow pattern, we could not clearly identify stop vortices at the end of each half stroke. In contrast, Saharon and Luttges (1988) described eight vortices that are shed into the wake of flapping dragonfly model wings: four vortices by each wing throughout the stroke cycle. The authors found that each simple element of wing motion, such as the transition from pitching to plunging motion, initiated its own vortex structure. Similar patterns are described for vortex shedding patterns in a 2D model wing (Savage et al., 1979). Savage et al. found that a LEV (first vortex) is initiated during wing translation, which is common in most insect model wings moving at high angle of attack and similar to the present study (Birch and Dickinson, 2001; Ellington et al., 1996). During wing rotation (supination) for the subsequent half stroke, a second vortex is shed from the trailing wing edge in conjunction with trailing edge vorticity (third vortex) left in the wake in order to satisfy the Kutta condition when the wing starts to translate (Savage et al., 1979). In most cases, these vortex structures are displaced in the 3D model in the horizontal direction or move downstream when reduced frequency (based on wing beat/plunging cycle) is increasing from 0.18 to 5.0 (Saharon and Luttges, 1988). In many instances, however, the changes in vortex travel velocity were small, suggesting that there might be only minor alteration in overall wake pattern when the animal is changing forward speed (or reduced frequency; Saharon and Luttges, 1988).

Second, in addition to that, the robotic model of Saharon and Luttges mimicked the dragonfly kinematics during escape mode found by Norberg (1975), which is characterized by a highly inclined stroke plane while the dragonfly body is held horizontal. The tilted stroke plane, in turn, requires that a large proportion of total lift is produced during the downstroke at which the angle of attack of the hindwing is close to 90°, whereas during the upstroke the wing flapped at 0° angle of attack (fig. 3 in Reavis and Luttges, 1988). Third, the kinematic pattern shown by Saharon and Luttges suggests that the robotic model rotated its wings rapidly at the stroke reversals, when translational wing velocity was approaching zero. This kinematic pattern exhibited rather discrete translational and rotational phases, and this might be the reason why these authors found that each simple element of wing motion, such as the transition from pitching to plunging motion, initiated its own vortex structure. In contrast, the onset of wing rotation in our model wing began 10% of the stroke period prior a stroke reversal and ended 10% after the stroke reversal, which resulted apparently in a combined shedding of vortices produced during wing rotation and translation.

*Changes in aerodynamic forces due to phase modulation*

Phase modulation effects on the forewing were small and only occurred in phase-shift cases where the fore- and hindwing were moving close to each other throughout the stroke cycle (Fig. 3D). Thus it seems likely that some of the modulation of forewing lift is caused by wall effects due to physical distortion of forewing downwash by the hindwing (Dickinson et al., 1999; Rayner, 1991). We measured the maximum increase in forewing lift compared to the performance of a forewing flapping separately from the hindwing, when the forewing leads by 2.5–5% of stroke cycle. In this case the forewing downwash is directed completely onto the dorsal surface of the hindwing throughout the stroke cycle (Fig. 5). However, at most kinematic phase shifts we measured a small decrease in forewing lift, although hindwing downwash effects on forewing lift should be considerably less than forewing downwash effects on hindwing lift (Fig. 6). Two effects might be responsible for this difference. First, downwash flow velocities are thought to be considerably larger

below a wing than above it (Demoll, 1918; Hoff, 1919). Because the wing accelerates flow downwards, the resultant flow below the wing will have a smaller cross-sectional area than the flow above it, according to Venturi's principle, and consequently the flow velocities in the region below the wing will be higher than above. Thus, the high flow velocities in the forewing wing downwash potentially influence hindwing lift to a greater extent than the low flow velocities produced by the hindwing influence forewing lift. Second, the vortical structures in the wake travel in the direction of the fluid jet acceleration and thus it is likely that vortices shed by the hindwing have less interaction with the forewing than *vice versa*. Nevertheless, the small but significant modulation in forewing lift disappears when the two wing hinges are separated by more than 5 wing chords, supporting our hypothesis that forewing lift modulation might be due to wall effects caused by the hindwing (Fig. 3B, open red circles).

In contrast to the forewing, the stroke-phase relationship between both wings alters hindwing lift production by a factor of approximately 2 (Fig. 3C). Quite similar to the finding on forewing lift, the modulation ceases when we increase the distance in vertical separation between the two wing hinges, resulting in an approximately constant loss of hindwing lift production (Fig. 10). This result suggests that the phase modulation of hindwing lift production is likely to be due to transient forewing wake structures, because at 5-chord-width depth the forewing wake velocities are rather

homogenized within the fluid. One potent transient vortex structure likely to influence hindwing lift is the forewing starting vortex that is left in wake while the traveling wing builds up aerodynamic circulation after starting from rest (Figs 5 and 6). Because of vortex interaction, we were not able to identify reliably the two vortices as single structures at all phases of the stroke cycle when flapping both wings; however, results obtained from so- called 'static' wing experiments might be able explain the relative decrease in leading edge vorticity of the hindwing, as shown in Fig. 8. We studied the potential threat of starting vortical structure on hindwing lift in DPIV experiments in which the hindwing remained static at its 15% of stroke cycle position throughout the forewing stroke (using identical fore- and hindwings, aspect ratio=3.6). These experimental conditions show that the position of the forewing's starting vortex is close to the hindwing's leading edge, next to the position of the developing LEV, potentially attenuating its development and thus decreasing hindwing lift.

The theoretical work by Lan (1979), who predicted that the optimum kinematics to maximize hindwing lift is a 25% phase shift, supports the finding in our physical dragonfly model but runs counter to lift measurements on a tethered flying dragonfly *Aeshna palmatta* (Reavis and Luttges, 1988). On the force balance, *Aeshna* (body weight 0.6 g) produces approximately
1.4 g lift when the 'beta angle' is ~87°. Reavis and Luttges (1988) defined the 'beta angle' as the angle between the freestream flow and the distance between the fore–aft wing tips. For this reason, the 'beta angle' is not identical with the phase-shift angle used in this study, although the 'beta angle' appears to be a comparable measure for the kinematic phase difference between the two flapping wings. The force measured in the animal *increases* to approximately 3.7 g lift when the 'beta angle' *decreases* to a value of approximately 52°, which appears to be opposite to the finding in our dragonfly model. Nevertheless, the tethered flight data apparently indicate that a change in kinematic phase relationship between the fore- and hindwing may modulate total peak lift by a factor of 2.6. This value is approximately twice the modulation we found in the present study for the performance of the combined wings (Fig. 3D) and is close to the modulation we found for the hindwing (Fig. 3C). A possible explanation for the discrepancy in sign between the data derived from the dragonfly and the analytical/physical model is that while varying phase shift, the dragonfly modulates simultaneously other kinematic parameters such as stroke amplitude (varies in the hindwing between 60 and 75°), stroke frequency (varies between 34 and 37 Hz) and maximum angle of attack of both wings (forewing range is 65–90°, hindwing range is 35–55°; Reavis and Luttges, 1988). Since the force data derived from the tethered dragonfly imply that maximum lift increases linearly with an increase in all three kinematic parameters, a phase advance of the hindwing, in conjunction with a pronounced *decrease* in amplitude, frequency and/or angle of attack, would explain the decrease in lift measured in the tethered flying animal.

*Regain of hindwing lift*

Despite vortex interaction in the wake produced by the combined fore- and hindwing downwash it is remarkable that the hindwing, whilst flapping in the wake of the forewing, is able to restore lift to a level close (within 2.5%) to that of the hindwing flapping free from forewing downwash. Although this can only be achieved at a flapping condition where the hindwing motion leads by a quarter stroke cycle, it is quite unexpected because recent studies have shown that for two- winged hovering insects the first wingbeat produces more lift than subsequent wingbeats (Birch and Dickinson, 2001). A likely explanation of this finding is that the first stroke moves through undisturbed air and all subsequent strokes move through the downwash of the previous stroke, which may reduce lift by more than 10% (Birch and Dickinson, 2001). The same phenomenon is found in helicopter aerodynamics, where each rotor blade passes through the downwash generated by the preceding blade (Stepniewski and Keys, 1984). Closely related to helicopter technology (single and coaxial rotor blades) is the counter-rotating propeller technology (tandem propeller) in some long-range reconnaissance aircrafts such as the Shackleton. At small forward speeds, a single propeller imparts a significant amount of rotational flow to the air passing through the propeller disk. This rotational flow does not contribute to thrust, and lowers the lift-to-drag ratio and thus the efficiency of the aircraft. A second propeller close to the first propeller and turning in the opposite direction, however, may turn the rotational motion of the fluid into useful thrust, which appears to be widely related to the fluid dynamic

phenomena found in our root flapping dragonfly wings. Our direct force measurements show that the regain in hindwing lift in the dragonfly model results from a complex temporal pattern in which hindwing lift is attenuated at the early stroke phase (15% of stroke cycle) but then produces lift in excess of that produced by a wing flapping separately later in the half stroke cycle (35% of stroke cycle).

The estimates of wing inertia and added mass inertia as shown in Fig. 2 suggest that the alterations in hindwing lift are not easily attributable to inertial components because those components are typically less than 5% of the measured force. For this reason, it appears more likely that the changes in hindwing lift result from aerodynamic phenomena rather than from pronounced inertial effects. Thus to understand the nature of hindwing lift attenuation and enhancement for the best phase case in more detail, we estimated both leading edge vorticity and the local flow conditions, because lift depends on fluid velocity and circulation (Ellington, 1984b). At the early stage in the half stroke (at 15% of hindwing stroke cycle), the small change in effective angle of attack from 2.1° to 1.6° might explain why hindwing lift (Fig. 4B, blue trace, *1) slightly decreases compared to a single hindwing, because LEV circulation would be similar (Fig. 9A,E, 51.7 *vs* 56.0 $cm^2$ $s^{-1}$). Despite the reasonable development of LEVs, the small effective angles of attack raise the question of why the model hindwing produces such large lift during wing translation. One possible explanation is that we underestimated the effective angle of attack because of leading edge vorticity. A translating wing that produces leading edge vorticity, causes the oncoming flow to behave as it does around a cambered wing. A cambered wing, however, is able to generate large lift even at low geometrical angle of attack close to zero. Although this view might explain the elevated flight forces early in the stroke cycle (Fig. 4A, *1), it cannot easily explain the *difference* in hindwing lift production during one- and two-wing flapping conditions because leading edge vorticity is similar in both cases, as mentioned above (Fig. 9A,E). Instead, it appears likely that in the flapping tandem wings, subtle static pressure distributions (especially the expected over pressure on the lower forewing surface) might attenuate hindwing lift, which was not estimated in the present study.

A similar aerodynamic mechanism to that described above (change in effective angle of attack) appears to apply later in the stroke (at 35% hindwing stroke cycle), at which lift increases above single wing performance due to an increase in angle and magnitude of the local flow of approximately 70% and 58%, respectively, compared to the single wing, while leading edge vorticity is approximately equal in both flapping conditions (123 *vs* 129 $cm^2$ $s^{-1}$; Fig. 9B,F). To explain the favorable gain in local flow conditions for the hindwing, we suggest the following hypothesis. Fig. 5 shows that the downwash produced by the wings is not directed exactly vertically downward because the inclined wings pull the fluid into the direction of wing motion (*re-actio* component of drag). As a consequence, at stroke conditions in which the hindwing faces the forewing downwash produced in a preceding subsequent halfstroke, the vector angle of the forewing downwash is less corruptive than the angle of the oncoming fluid when both wings translate in the same direction (Fig. 9C). The hindwing in Fig. 9F thus yields a high angle of incidence towards the oncoming flow (28.5°) because the local downwash is determined partly by the forewing downwash produced in the previous forewing halfstroke (cf. inclination of green arrows in Fig. 9). In addition to that, the velocity of the forewing downwash contributes to the flow velocity that the hindwing experiences while moving through the fluid, which in turn amplifies aerodynamic force production at this moment of the stroke cycle (Fig. 4B). Assuming that this explanation is valid, then we would also expect a favorable downwash at 35% downstroke cycle when the forewing leads wing motion, because at this moment the forewing downwash is thought to be directed similarly towards the hindwing (Fig. 9D). The reconstruction of local flow conditions, however, has shown that under these flow conditions the local flow vector points into the direction of the hindwing downwash (green arrow points in the direction of hindwing motion) and thus lowers the hindwing's effective angle of attack (Fig. 9D). A possible reason for this phenomenon is that the LEV on the forewing is not fully developed at this moment of the stroke, indicated by the small decrease in total lift at 25% kinematic phase lag (Fig. 3B). Therefore, we suggest that the decrease in aerodynamic performance of the forewing at 35% stroke cycle, due to a possible reduction in leading edge vorticity, might lower the hindwing's capability to produce lift because of unfavorable local flow conditions. We further assume that this hindwing–wake interaction might be highly sensitive to subtle changes in stroke kinematics that alter leading edge vorticity at the beginning of the stroke cycle, such as timing and speed of wing rotation during the ventral and dorsal stroke reversals. The dependency of hindwing lift modulation on stroke cycle timing, as shown by our generic kinematic model, might even indicate that by adjusting more kinematic parameters in the stroke cycle, a higher gain in lift performance might be achieved than the one shown here.

*Wing–wake interaction between contralateral wings*

The small stroke amplitude of typically 50–100° found in flying dragonflies limits the interaction of flow structures produced by the ipsilateral and contralateral wings because the biofoils are well separated during ventral and dorsal stroke reversal (Alexander, 1982, 1984, 1986; Azuma and Watanabe,
1988; Chadwick, 1940; Norberg, 1975; Reavis and Luttges,
1988; Rudolph, 1976a,b; Rüppell, 1985, 1989; Wakeling and Ellington, 1997; Weis-Fogh, 1967). High-speed film sequences of tethered flight kinematics in dragonflies show only one example in which the dragonflies *Libellula luctosa* and *Celithemis elisa* performed a physical interaction between the wings during the dorsal stroke reversal (Alexander, 1984). However, unlike dragonflies,

damselflies typically show dorsal wing interaction and may use an unsteady lift enhancing mechanism termed the clap-and-fling or partial fling (Rudolph, 1976a,b; Wakeling and Ellington, 1997). For example, the damselfly *Calopteryx splendens* performs the clap-and-fling similar to the motion of the wings described by Weis-Fogh (1973) for the small wasp *Encarsia formosa*. As the wing reaches the top of the upstroke, the upper wing surfaces meet and then, as the wings rotate and separate, air is drawn into the opening gap, enhancing wing circulation and thus wing lift (Bennett, 1977; Edwards and Cheng, 1982; Ellington, 1975; Lighthill, 1973; Maxworthy, 1979; Spedding and Maxworthy, 1986; Sunada et al., 1993; Weis-Fogh, 1973). In addition to damselflies, the clap-and-fling was found in various other insect species such as various Diptera (Ellington, 1984b; Ennos, 1989), lacewings (Antonova et al., 1981) and a whitefly (Wootton and Newman, 1979). It has been shown that insects performing clap-and-fling wing motion produce 25% more muscle mass-specific lift than insects flying with conventional wing beat (Marden, 1987). The clap-and-fling mechanism is not modelled by our generic kinematics for dragonfly because we employed solely two ipsilateral wings. Besides the clap-and-fling, a contralateral wing might also influence force production and thus phase-shift modulation of lift on an ipsilateral wing *via* the extension of LEV over the midline of the animal. This has been demonstrated in the red admiral butterfly *Vanessa atlanta*, flying freely in a wind tunnel with a free stream velocity at around 1–2 $m\ s^{-1}$ (Srygley and Thomas, 2002). At the moment of take-off, the body angle of the animal with respect to the oncoming air and the wing's angle of attack approaches high values, supposedly inducing flow separation on the dorsal side of the body. As a consequence, the separation bubble on the dorsal body surface might facilitate the LEVs of both wings to expand over the body midline towards the contralateral wing. It remains open whether the qualitative description of flow pattern in the butterfly can be necessarily carried across to hovering flight in dragonflies at zero advance ratio, because under these conditions the wing root and the body of the animal only face the downwash that is orientated downwards and thus would be likely to initiate flow separation on the lower side of the animal's body. The high body angle and the relatively high flow velocity in the wind tunnel might, in case of the butterfly, provide an explanation for why the expansion of a LEV across the midline was not described in physical models that mimic hovering flight conditions in insects so far.

### *Concluding remarks*

The present study on kinematic phase relationship in a hovering dragonfly model suggests that under certain kinematic conditions, lift production in tandem wings is maximized when the hindwing leads wing motion by approximately a quarter stroke cycle. It is possible that this result only holds for a limited range of wing kinematics and is limited to hovering flight conditions, although systematical variations in forward speed (reduced frequency) of the larger dragonfly model of Saharon and Luttges (1988) did not produce significant changes in flow structures. Additional flow components due to fast forward flight potentially influence local flow conditions, vortex initiation and vortex travel

velocity in the wake produced by the wings (Wang, 2000a,b). To evaluate the robustness of our findings to changes in forward flight speed or reduced frequency, we simulated changes in vortex travel velocity by varying the vertical separation of the two wing hinges. The results in Fig. 10 show that the optimum phase relationship between two model wings (maximum hindwing lift) decreases with increasing distance between the two wings (peak force moves to the left). A possible explanation for this phenomenon is that the duration between the time at which the forewing sheds vortices and when those vortices interfere with the hindwing is increasing with increasing distance between the wings. This result implies that any change in stroke-phase relationship must be seen at least in conjunction with the magnitude of wing separation, because both kinematic parameters appear to determine the best phase for lift production in the tandem wing. The finding that the travel velocity of some vortices also depends on phase relationship (hindwing phase leads produces faster travel velocity due to an increase in downwash velocity) at constant wing separation might even complicate the aerodynamic consequences of the two kinematic parameters (Saharon and Luttges, 1989).

A similar picture might appear for aerodynamic effects due to more subtle changes in wing kinematics such as wing torsion, flexing, and changes in wing camber during flight (Song et al., 2001; Sunada et al., 1998), including effects due to corrugation of dragonfly wings (Kesel, 2000). Wing flexing, for example, has been discussed as a modification of the clap- and-fling termed the 'clap-and-peel', which might alter force production during the fling part of the wing motion (Ellington, 1984b). This modified clap-and-fling kinematics was found in fixed flying *Drosophila* (Götz, 1987) and larger insects such as butterflies (Brackenbury, 1991a; Brodsky, 1991), bush cricket, mantis (Brackenbury, 1990, 1991b), and locust (Cooter and Baker, 1977). In contrast, in our dragonfly model we used rigid flat plates that deformed only slightly during wing translation or wing rotation (Fig. 1D). Studies on the aerodynamic characteristics of dragonfly, for example, show that corrugated wings may have a slightly higher lift coefficient under 2D conditions than flat plates (Kesel, 2000; Okamoto et al., 1996). In sum, we have shown that by using a generic stroke pattern derived from dragonfly kinematics, the phase relationship between a robotic fore- and hindwing may modulate hindwing lift force due to two separate, though not independent, effects. One seems to be the attenuation of hindwing leading edge vorticity (LEV destruction), and the second is the speed and angle of local flow conditions. The hindwing leading edge vorticity seems to be dependent upon hindwing proximity to the forewing starting vortex, the wing

position within the stroke cycle and the local flow conditions. Timing between the fore- and hindwing can modulate the wake interference effects and can achieve instantaneous lift force greater than that achieved by a wing free from wake interference. The small decrease in lift-to-drag ratio does not necessarily imply that there is a small energetic cost associated with having two pairs of wings, because profile costs depend on the product between wing velocity and drag (Fig. 3D). This issue of the fluid dynamics in four-winged insects we will address in a subsequent paper on the power requirements and aerodynamic efficiency of root-flapping tandem wings. The major benefit from the ability to modulate forces through fore- and hindwing phase relationships might be that it allows an insect to control lift production without further changes in stroke kinematics, thus offering an additional parameter for flight control. As suggested by several previous studies, right–left asymmetry in phase shift might allow functionally four-winged insects the ability to modulate forces asymmetrically, and this might explain why many dragonflies have been reported to vary phase shift during some turning maneuvers (Alexander, 1986; Norberg, 1975; Reavis and Luttges, 1988; Rüppell, 1989).

## Reference s


According to Alexander, D. E. (1982). Analyses of Dragonfly Flight Control and Aerodynamics. Durham, NC: Duke University.

Author(s): Alexander, David E. (1984). When it comes to dragonflies in flight, the forewings and hindwings have some strange phase correlations. Published in: Journal of Experimental Biology 109, pages 379–383.

Author: Alexander, David E. (1986). Research on dragonfly wing twists in a wind tunnel.

Publication information: J. Exp. Biol. 122, pp. 81–98.

O. A. Antonova, A. K. Brodsky, and V. D. Ivanov (1981). The kinetics of five different insect wing beats. Zool. Zh. 60:506–518, 2000.

We thank Azuma and Watanabe for their contributions (1988). How well a dragonfly flies. J. Exp. Biol. 137:225–252.

We thank Azuma, S. Azuma, Watanabe, I., and Furuta, T. (1985). Dragonfly flight dynamics. 116, 79–107 in the Journal of Experimental Biology.

The authors' names are Baker, P. S., and Cooter, R. J. (1979). Locusta migratoria L., or the migratory locust, has a unique and beautiful wingbeat that is used in its natural flying. The Journal of Comparative Physiology 131:79–87.

L. Bennett (1977). Experimental analysis of the aerodynamics of the clap-and-fling technique. Journal of Experimental Biology, Volume 69, Issue 2, Pages 261–272.

John L. Bertin and Michael L. Smith (1979). Engineers' Guide to Aerodynamics.

Printed by Prentiss-Hall, Inc. in Englewood Cliffs, New Jersey.

J. M. Birch and M. H. Dickinson (2001). The leading-edge vortex and its relationship to the span of insect wings. Nature 412:729–733.

It was Brackenbury (J. (1990). The bush cricket, Tettigonia viridissima, and the mantis, Ameles spallanziana, both use their wings in a specific way as they jump in nature. To cite this article: J. Zool. Lond. 220, 593-602.

Authors: Brackenbury, J. (1991a). The kinetics of butterfly takeoff and ascent. 224:251-270 in J. Zool. London.

I. Brackenbury (1991b). The wing kinematics of the religious and oratorical mantids, Mantis religiosa and Iris oratoria, respectively, during their respective natural-leaping behaviors. Zool. J. (London) 223:341–356.

To cite this work: Brodsky, A. K. (1991). Several features of the development of insect flight, as well as the production of a vortex during the tethered flight of the peacock butterfly Inachis io L. (Lepidoptera, Nymphalidae). J. Experimental Biology 161:77–95.

By L. E. Chadwick (1940). The flapping of a dragonfly's wings. 35, No. 109–112 in Bulletin of the Brooklyn Entertainment Society.

L. E. Chadwick (1953). Flight action, or wing motion. Pages 577–614 in Insect Physiology (ed. K. D. Roeder). John Wiley & Sons, Inc., New York.

Mr. Clark, H. W. (1940). Muscles of the thorax in an adult anisopterous dragonfly (Odonata, Anisoptera). Journal of Morphology, 67:523-565.

As authors, R. J. Cooter and P. S. Baker are credited (1977). Locusta uses the Weiss-Fogh clap-and-fling mechanism. Science 269, pp. 53–54.

R. Demoll & J. (1918). Animals and birds taking to the air. Dickinson, M. H., F.-O. Lehmann, and K. G. Götz. Jena: G. Fisher (1993). Drosophila's ability to actively regulate wing rotation. Journal of Experimental Biology, 182(173):173-189.

According to the research of Dickinson, M. H.; Lehmann, F.-O.; and Sane, S. (1999). Bugs can fly because of the spinning of their wings and the air resistance they create. The scientific journal "Science" 284:1954–1960.

According to Edwards, R. H., and Cheng, H. K. (1982). A key component of the process that creates Weiss-Fogh circulations is the separation vortex. 463-473 in J. Fluid Mech.